Int. J. Heat Mass Transfer. Vol. 25, No. 6, pp. 871–887, 1982
Printed in Great Britain

0017-9310/82/060871-17 $03.00/0

EXPERIMENTAL INVESTIGATION OF TURBULENT WALL-JETS IN THE PRESENCE OF ADVERSE PRESSURE GRADIENTS IN A RECTANGULAR DIFFUSER

LLOYD BACK and ROBERT CUFFEL*
Jet Propulsion Laboratory, Pasodenia, CA 91103, U.S.A.

(*Received* 10 *December* 1981)

Abstract—An experimental study of wall static pressure distributions and mean velocity profiles along a duct and diffuser downstream of wall-jet injection was conducted over a range of diffuser total angles from 15 to 40° at injection to core flow mass flux ratios from 0 to 6. Pressure recovery in the diffuser increased with injection ratio and decreased with diffuser total angle. Peak velocities in the wall-jet decayed along the flow and the inner shear layer and outer mixing region grew in thickness along the flow. The inner layer was near similarity condition, but non-similar variations were found in the outer layer. Estimated wall shear stresses depended upon injection mass fluxes, downstream distance and diffuser total angle. Greater decay of peak velocity and larger friction coefficients were found in the diffuser than indicated by correlations from data for a wall-jet without a pressure gradient. At the largest diffuser total angle and the highest injection ratio flow reversal occurred in the core region.

NOMENCLATURE

- c_f, friction coefficient;
- c_p, pressure coefficient;
- l, distance between the effective origin of the jet and injection slot;
- m, injection ratio, $\rho_j U_j/\rho_0 U_0$;
- p, static pressure;
- p_{to}, stagnation pressure;
- s, slot height;
- u, velocity component parallel to wall;
- u_e, minimum velocity in outer portion of wall-jet;
- u_m, peak velocity in wall-jet;
- u_r, centerline velocity or at data point furthest from wall;
- $u_{1/2}$, velocity midway between u_m and u_e;
- u_τ, friction velocity, $(\tau_w/\rho)^{1/2}$;
- u^+, dimensionless velocity, u/u_τ;
- U, bulk average velocity at injection slot location;
- x, distance along diffuser plate from end of duct;
- x_0, distance from injection slot to end of duct;
- $x + x_0$, distance along wall from injection slot;
- y, distance normal to wall;
- y^+, dimensionless distance normal to wall, $\rho u_\tau y/\mu$.

Greek symbols

- δ_e, distance normal to wall where $u = u_e$;
- δ_m, distance normal to wall where $u = u_m$;
- $\delta_{1/2}$, distance normal to wall where $u = u_{1/2}$;
- 2θ, diffuser total angle;
- μ, viscosity;
- ξ, distance downstream from the effective origin of the jet;
- ρ, density;
- τ_w, wall shear stress.

Subscripts

- j, condition at injection slot face;
- 0, condition in core flow at injection slot location;
- r, condition at first pressure tap in diffuser.

*Present address: Walla Walla College, WA 99324, U.S.A.

1. INTRODUCTION

INTERIST in ejector-type thrust augmentors for military aircraft dates back to the early 1960s with the goal of achieving thrust augmentation ratios of 2.0, which later was reduced to 1.4–1.5. Subsequent testing on full scale aircraft produced ratios of only 1.0–1.1 even though small scale and component tests were more promising. Important in this regard is a basic understanding of the fluid mechanics phenomena associated with entrainment of the secondary fluid and its mixing with the primary injection. Two modes of primary injection are center jets and coanda jets along the walls.

An experimental investigation has been conducted at the Jet Propulsion Laboratory on the structure of planar turbulent wall-jets in regions of adverse pressure gradients in a rectangular diffuser. In this paper mean flow data are presented including pressure recovery in the diffuser, velocity profile shape and variation, spreading of the wall-jet, decay of the maximum wall-jet velocity, and wall shear stresses. In the experiments the diffuser total angle 2θ was varied from 15 to 40° (14.8, 24.9 and 39.9 total angles were used) at injection ratios $\rho_j U_j/\rho_0 U_0$ from 0 to about 6.

The experimental apparatus, instrumentation and operating conditions are described in Section 2, the experimental results are reported in subsequent Sections 3, 4 and 5, and summarized in Section 6.

Turbulent wall-jets have been investigated extensively since the early work of Glauert [1] and have practical application in film cooling (e.g. the survey by Goldstein [2]) and in boundary layer control. There is less data on turbulent wall-jets confined in duct flows with adverse pressure gradients; e.g. the discussion and measurements in conical diffusers by Ramaprian [3].

2. EXPERIMENTAL APPARATUS, INSTRUMENTATION AND OPERATING CONDITIONS

The experimental apparatus, shown schematically in Fig. 1, consisted of an inlet duct, test section, downstream diffuser and blower. Ambient air at 296 K and 0.959 atm. was drawn through the apparatus by the blower and exhausted at the other end of the room. The duct inlet was rounded somewhat at the entrance lip. To reduce core flow turbulence fluctuations so that meaningful pitot tube measurements could be made in the outer portion of the wall-jet, upstream trips and screens at the duct inlet section were not used. The duct surface was smooth.

The inlet duct was 12.7 cm high, had an aspect ratio of 4, and extended 107.5 cm upstream of the injection slot. Although the inside height of the inlet duct varied along the flow path, the channel width did not change up to the downstream diffuser. The inside height gradually decreased along a distance of 7 cm before the injection slots to allow for the two, 0.196 cm high injection slots, one on top, the other on the bottom. Downstream of the slots the duct height was 12.78 cm, and the duct continued a distance of $x_0 = 14.12$ cm downstream of the injection slots. The straight diffuser plates on the top and bottom fitted flush to the end of the duct and pivoted on a 0.952 cm corner radius to provide the various divergent angles tested.

The flow along the lower half of the test section was investigated (Fig. 2). The lower plates of the duct and diffuser contained 0.51 mm dia wall static pressure taps at 2.54 cm intervals along the wall. The upper plates contained slots along the centerline and parallel to the injection slot (just downstream of the injection slot) through which probes were inserted. The pitot tube was made from a 0.108 cm O.D. tube that was flattened and filed to a 0.15 mm tip height. The pitot tube was traversed normal to the wall and was inclined 5–10° toward the wall to ensure that the tip touched the wall. The inclination of the pitot tube permitted measurements in the outer region of the shear layer even with the largest total angle of the diffuser since pitot tubes are relatively insensitive to yaw up to angles of 10–15° [4, 5]. A larger tube formed the shaft of the pitot probe to provide rigid support. The total pressure along the centerline was measured with a 0.32 cm O.D. tube just downstream of the slot as indicated in Fig. 2. This tube which indicated negligible spanwise variation in total pressure was moved to one side during the pitot tube surveys.

Differences between wall static pressure tap readings, pitot pressure, and atmospheric pressure were obtained with oil manometers. The traversing pitot tube pressure was measured with a $\pm$ 7 kPa ($\pm$ 1 psi) differential transducer relative to a wall static pressure tap upstream and recorded continuously across the flow on an x–y plotter vs distance normal to the wall. The wall location was determined by electrical contact and the probe location was determined with a helipot attached to the motorized drive screw mechanism. Traverses were made from the wall to the centerline for cases where this distance was within the maximum allowable traversing distance of 13 cm. Otherwise, the traverses were terminated at 12 cm. In the data reduction, the static pressure was assumed to be constant across the flow normal to the wall at the measured wall value. The total temperature was assumed to be that of the ambient air outside of the duct inlet which was measured with a thermocouple. Compressibility effects were taken into account in the data reduction by assuming the total temperature to be invariable across the shear layer since the wall was essentially adiabatic. A value of the specific heat ratio $\gamma = 1.4$ was used.

Six or seven pitot tube traverses were made across the flow at various distances downstream from the injection slot at most of the combination of injection ratios and diffuser angles studied. These traverses were made at two locations along the flow in the duct between the injection slot and the diffuser plate at distances $x + x_0$ of 5.2 and/or 10.3 cm. Note that x is distance measured along the diffuser plate from the end of the duct (Fig. 1) so that values of $x + x_0$ in the duct or diffuser are distances along the wall measured from the injection slot. Traverses were made at five or six locations along the diffuser plate where the cor-

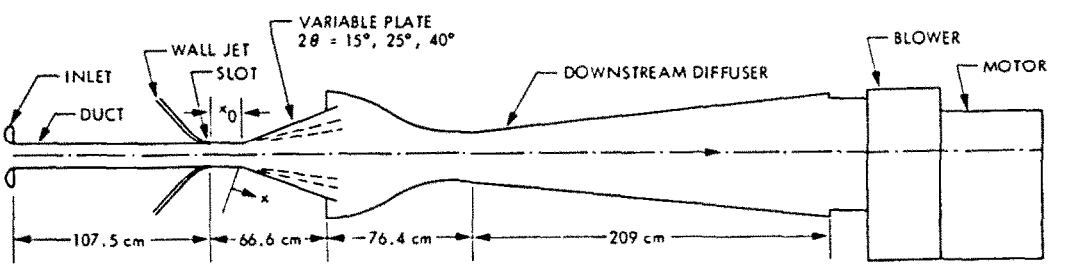

FIG. 1. Experimental apparatus.

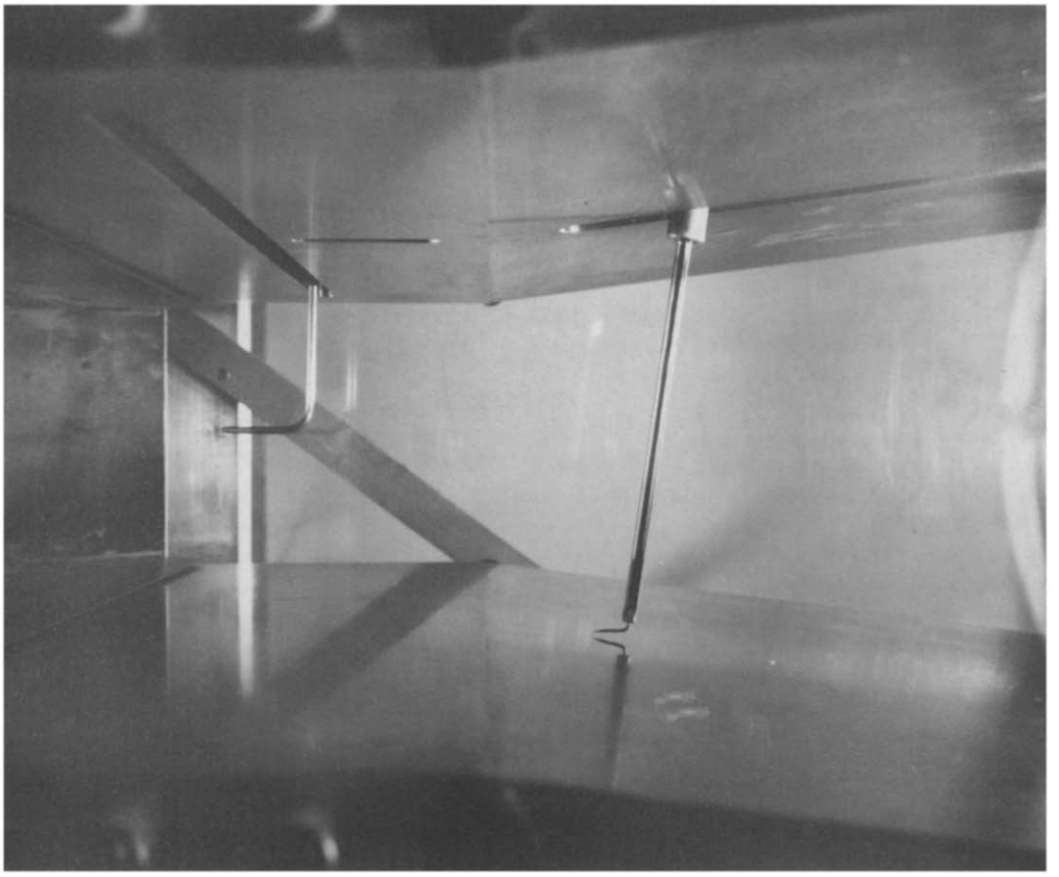

FIG. 2. Test section and probes.

responding distance $x + x_0 = 14.1$ cm. Average values from the six pitot tube traverses at each location were used in the data reduction.

The injection ratios $\rho_j U_j / \rho_0 U_0$ were obtained from measured mass flow rates and appropriate flow cross-sectional areas. The total mass flow rate $\dot{m}_t$ through the half-height of the duct was obtained from the pitot tube traverse nearest the injection slot at $x + x_0 = 5.2$ cm. The mass flow rate $\dot{m}_j$ of the wall-jet was measured with an orifice in the pipe far upstream of the injection slot where air was supplied at 297 K. The mass flow rate $\dot{m}_0$ in the core flow was then obtained by subtracting the mass flow rate in the wall jet from the total mass flow rate. The injection ratios were then

$$m = \frac{\rho_j U_j}{\rho_0 U_0} = \frac{(\dot{m}_j / A_j)}{(\dot{m}_0 / A_0)} \tag{1}$$

where A_j is the injection slot cross-sectional area, and A_0 is the product of the half-height of the duct minus the slot height, multiplied by the duct width. Injection ratios of 0, 2.3 and 5.9 were primarily investigated by traverses at the six or seven locations along the flow mentioned previously. A single pitot tube survey was obtained near the end of the diffuser plate at intermediate injection ratios of 3.3, 4.3 and 5.2.

Core flow velocities U_0 near the injection slot ranged from 36 ms^{-1} with no injection to 40.1 ms^{-1} at the highest injection ratio of 5.9. This increase in core flow velocity with increasing injection rates was presumably induced by the wall-jet. The core flow velocities were low enough for compressibility effects to be negligible in the core flow. This was not the case, however, for the injectant air for injection ratios above 3. Peak Mach numbers in the wall-jet at the traversing stations in the duct were less than 0.5 at the highest injection ratio of 5.9.

Qualitative flow observations were made with a row of yarn tufts attached to the upper and lower walls of the diffuser at one side.

Because of the large amount of data obtained, a portion of the data is not shown at the smallest and largest diffuser total angles of 14.8° and 39.9°, respectively. However, reference to the data for the smallest and largest diffuser total angles is included in the text in discussing the 24.9° total angle results shown.

3. WALL STATIC PRESSURE MEASUREMENTS AND RECOVERY

Wall static pressures normalized by the stagnation pressure are shown along the duct and diffuser downstream of the slot in Fig. 3 at a diffuser total angle 2θ

of 24.9. These measurements represent average values for about six tests at each operating conditions. Downstream of the slot and before the diffuser, the wall static pressure decreased presumably because of the upstream influence associated with the corner at the diffuser entrance. In this region, local flow accelerations occurred. With no injection, the core flow is believed to have separated from the wall downstream of the slot and reattached upstream of the first static pressure tap at $x + x_0$ of 2.7 cm, or 14 slot heights downstream of the slot. For the highest injection ratio of 5.9 there was a local static pressure rise and then a decrease again in the duct at the two larger diffuser angles. The reason for this is not clear. The static pressure continued to decrease along the wall as far as the vicinity of the corner region at the diffuser entrance, the decrease being greatest at the highest injection ratio. In the diffuser the static pressure increase associated with the flow deceleration was greatest at the highest injection ratio. The static pressure distributions tended to level out more quickly in the diffuser at the larger total angles. In particular at the largest total angle, the static pressure subsequently decreased with the distance along the wall at the higher injection rates (Fig. 4).

The implication of this latter behavior at the largest total angle and at higher injection rates is discussed subsequently in connection with the pitot tube measurements and some flow observations in Section 4.

The wall static pressure distributions in the diffuser are shown in Fig. 4 for all the diffuser total angles in terms of the pressure coefficient

$$c_p = \frac{p - p_r}{(1/2)\rho_r U_r^2} \tag{2}$$

where the subscript r refers to the condition at the first tap in the diffuser. As was also evident in Fig. 3, the pressure recovery increased with injection ratio. The dashed curve shown in Fig. 4 is a reference curve for pressure recovery for idealized 1-dim., inviscid, incompressible core flow as determined from a momentum balance between the first tap in the diffuser and subsequent downstream locations. Clearly, large deviations occurred from such a simple relationship even with no slot injection, the variations being greater at the larger diffuser total angles.

4. MEAN VELOCITY PROFILES, CHARACTERISTIC VELOCITIES AND THICKNESS

For subsequent reference, characteristic velocities and thicknesses in wall-jets are shown diagrammatically in Fig. 5. The distance normal to the wall where the peak velocity u_m occurs in the wall-jet is denoted as δ_m. Since the location denoted as δ_c for the minimum velocity u_c is generally not well defined, the distance $\delta_{1/2}$ is used which is associated with the local velocity denoted by $u_{1/2}$. This velocity is midway between u_m

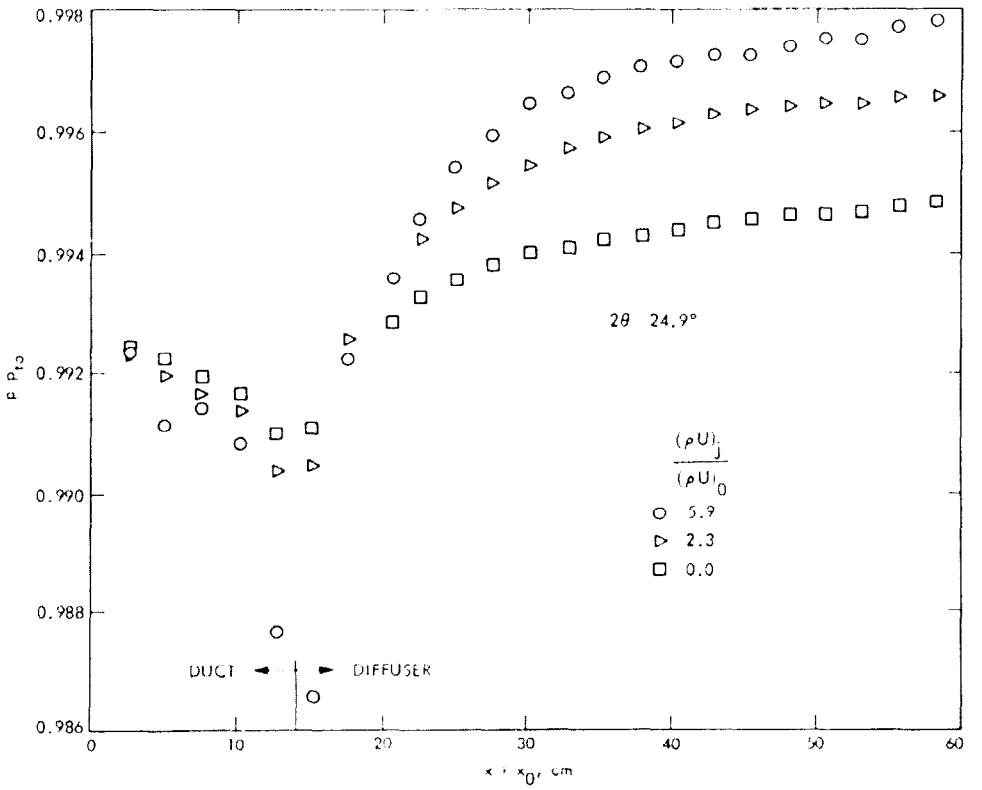

FIG. 3. Wall static pressure distributions, $2\theta = 24.9°$.

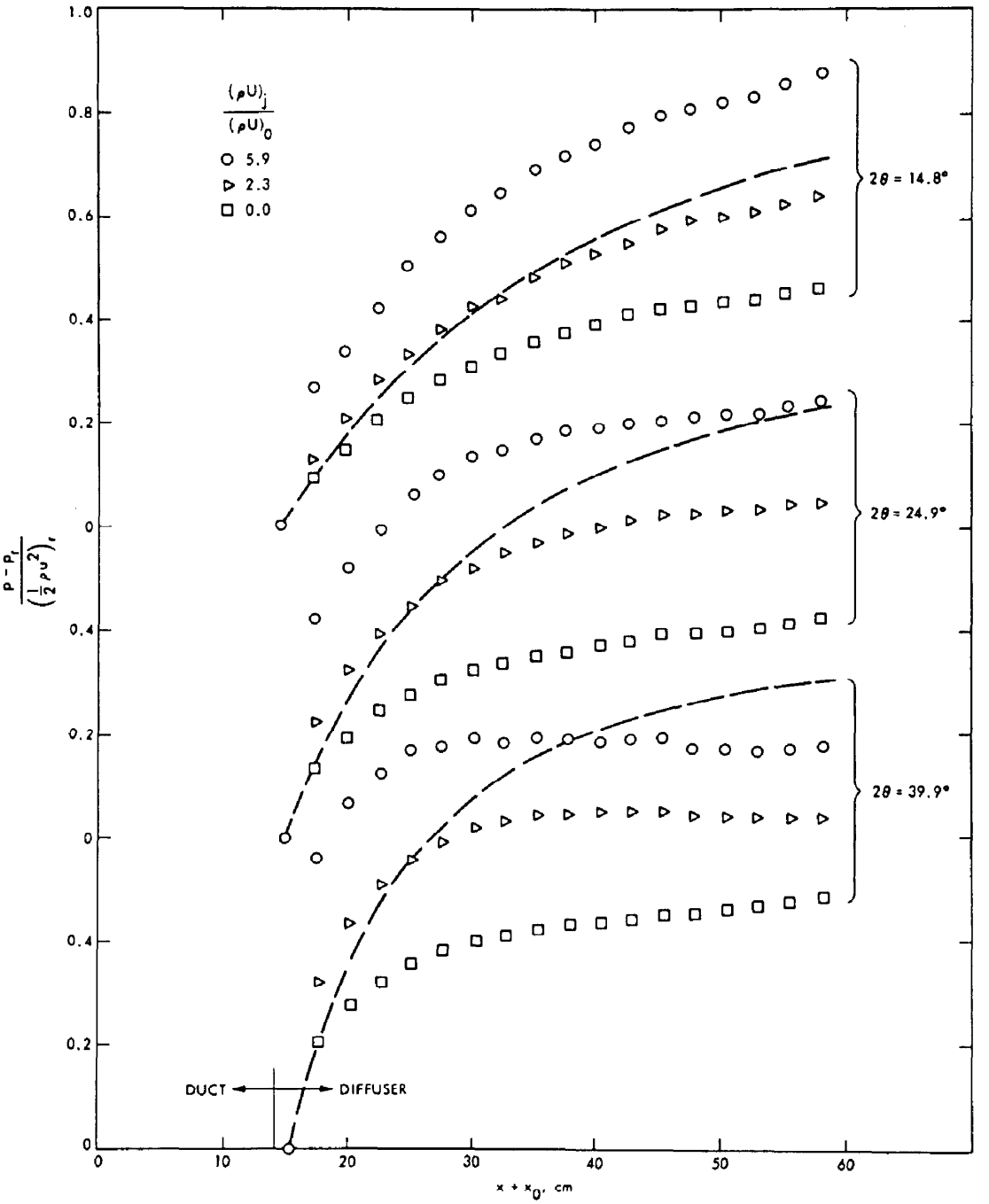

FIG. 4. Pressure coefficients in the diffuser, 2θ = 14.8, 24.9 and 39.9°. The dashed curve is for inviscid flow.

and u_e. The characteristics u_m are descriptive of the shear layer adjacent to the wall, and the characteristics $u_{1/2}$, $\delta_{1/2}$ are adjacent to the wall, and the characteristics $u_{1/2}$, $\delta_{1/2}$ are descriptive of the mixing region between the wall-jet and the outer flow. In the internal flow investigated herein, local velocities beyond δ_e either reached a plateau or gradually increased. The velocity profiles were non-dimensionalized by the value u_r at the data point farthest from the wall. This location was the lesser value of either the centerline location or a distance of 12 cm normal to the wall, as mentioned in Section 1.

Mean velocity profiles are shown in Figs. 6–8 over the range of injection ratios at a diffuser total angle of 24.9° at various locations along the flow. As mentioned previously, locations $x + x_0 = 5.2$ and 10.3 cm were in the duct between the wall-jet injection slot and the upstream edge of the diffuser plate, while locations $x + x_0 > 14.1$ cm were along the diffuser plate. Values of u_r are shown in parentheses on the figures when not evaluated at the centerline. With no injection (Fig. 6) the developing velocity profiles in the diffuser became

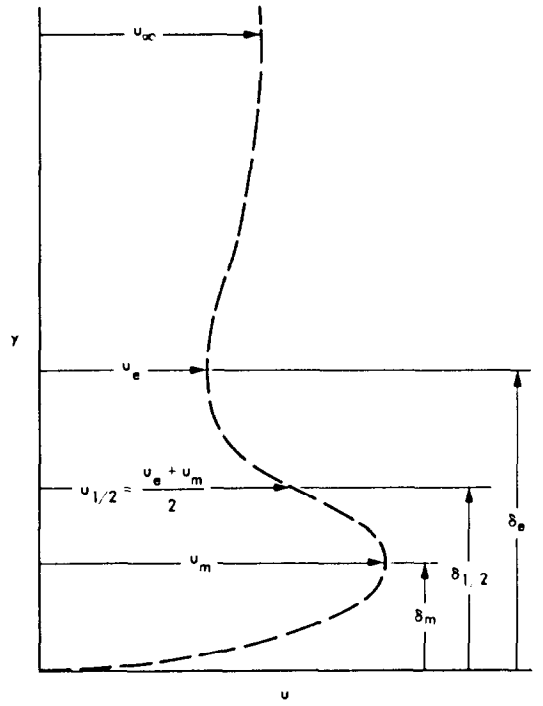

FIG. 5. Characteristic velocities and thickness in wall-jets (diagrammatic).

progressively distorted from the fuller profiles in the duct because of the adverse pressure gradient in the diffuser. The s-shaped profiles with no injection are more evident in a representation involving u^+ and y^+ which is discussed and shown subsequently (Section 5). With slot injection, the velocity profiles became peaked in the wall vicinity associated with the relatively larger injectant than core flow velocities. These peak velocities u_m then decayed along the flow, and the inner shear layer and the outer mixing region grew in thickness along the flow.

For the entire range of diffuser total angles and injection ratios the flow along the lower diffuser plate remained reattached in the wall vicinity as determined from the pitot tube traverses. At the largest total angle of $2\theta = 39.9°$ however, a different flow behavior occurred. With no injection, the row of yarn tufts attached to the upper and lower diffuser plates indicated that the flow separated from the upper diffuser plate, and that the entire flow followed along the lower wall, more or less steadily. The yarn tufts provide only qualitative information. A qualitative sketch of the asymmetric flow at this condition is indicated in Fig. 9(a). Also, at the largest total angle of $2\theta = 39.9°$, the measured pitot tube pressures were lower than the wall static pressures in the core flow at the highest injection ratio of 5.9. This indicated the pressure of reverse flow in the core region as shown in a qualitative way in Fig. 9(b). Note also that the wall static pressure decreased with distance along the latter part of the diffuser at this condition (Fig. 4). A more detailed study of the flow field for this condition would be required to learn about the actual behavior.

The variation of characteristic velocities along the flow is shown in Fig. 10 for total diffuser angles of $2\theta = 14.8$, 24.9 and 39.9°. Peak velocities u_m (open symbols)

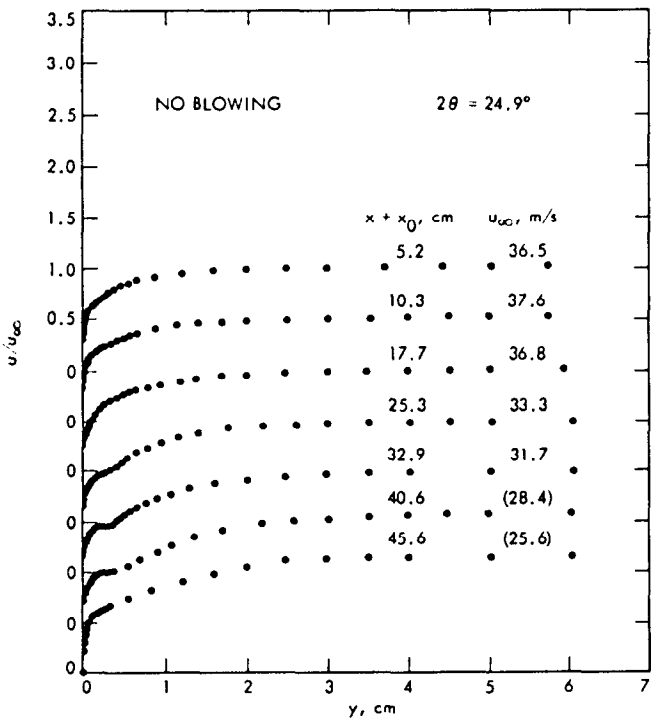

FIG. 6. Velocity profiles along the flow, $2\theta = 24.9°$, $m = 0$.

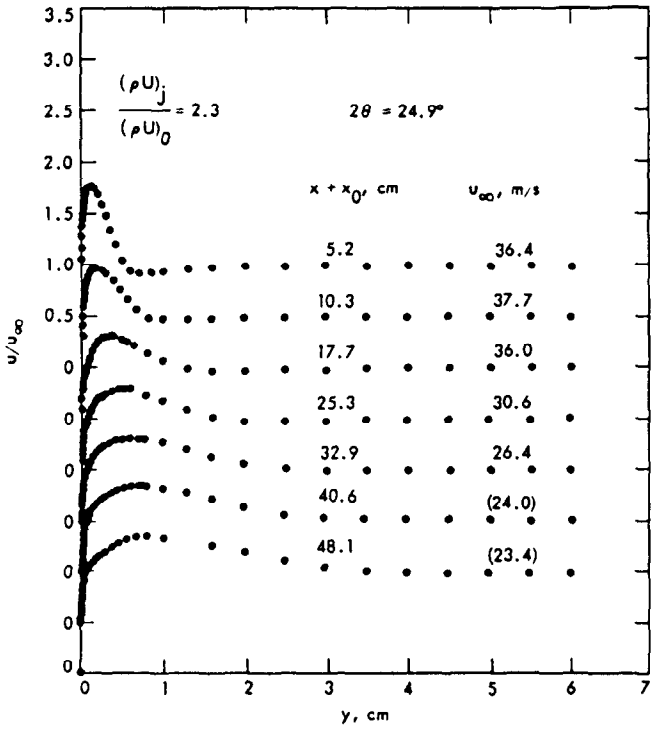

FIG. 7. Velocity profiles along the flow, $2\theta = 24.9°$, $m = 2.3$.

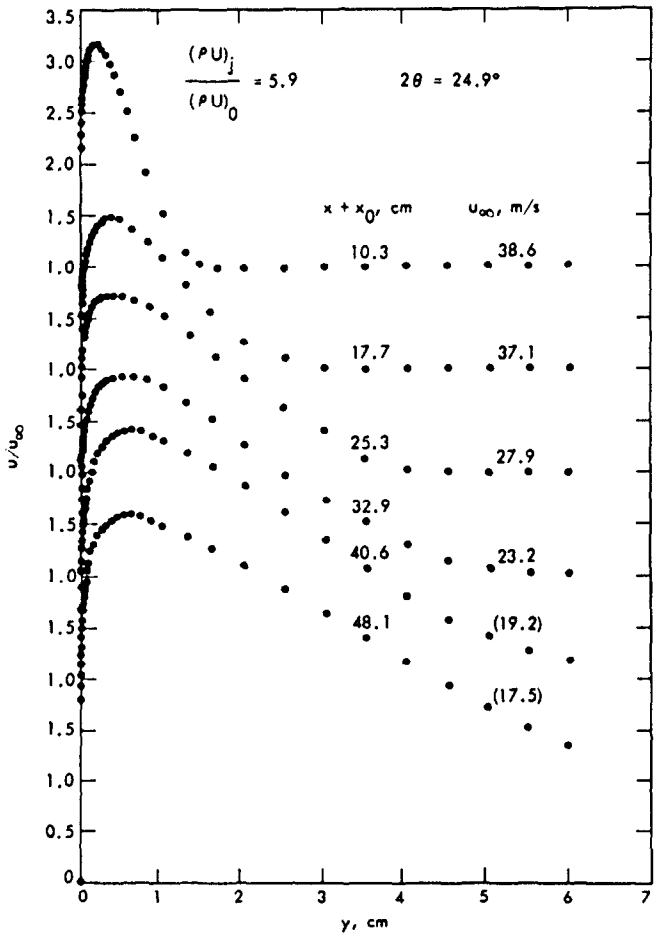

FIG. 8. Velocity profiles along the flow, $2\theta = 24.9°$, $m = 5.9$.

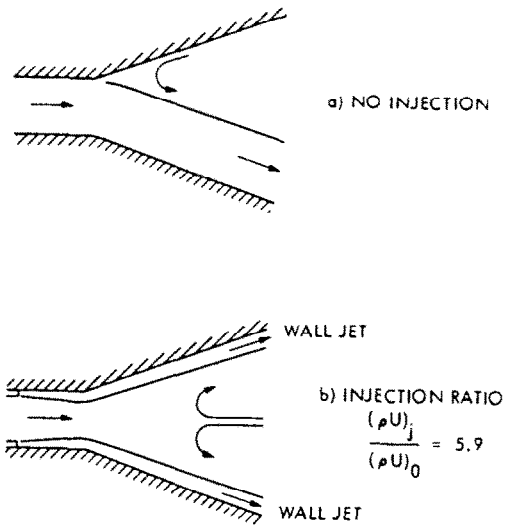

FIG. 9. Qualitative flow fields for diffuser total angle $2\theta = 39.9°$.

decayed with distance from the injection slot in a near power law manner that was observed to be independent of the total diffuser angle. Note that the lines shown in the figure are all the same at a given injection ratio. The dependence was of the form

$$u_m \propto (x + x_0)^{-\alpha} \tag{3}$$

with the exponent being only slightly different for the two injection ratios, i.e. for the larger injection ratio $m = 5.9$, $\alpha = 0.44$ and for $m = 2.3$, $\alpha = 0.40$. This indicates that at these injection ratios the relative decay of the wall-jet did not depend upon change in flow direction nor deceleration imposed by the diffuser. In section 5, scaling involving normalization of the peak velocity by the injection velocity; i.e. u_m/U_j and distance from the slot by slot height; i.e. $(x + x_0)/s$ is discussed. As is evident in Fig. 10, minimum velocities u_e (u_∞ for no injection), solid symbols, remained relatively constant in the duct and then decreased along the diffuser because of core flow deceleration.

The variation of the inner layer thickness δ_m at which peak velocity u_m occurred is shown in Fig. 11 for total diffuser angles of $2\theta = 14.8$, 24.9, and 39.9°, respectively. The results show that the growth of the inner layer thickness was essentially linear with distance along the wall from the injection slot, and was invariable with the injection ratio and the diffuser total angle; i.e. the lines shown in the figure are all the same. The angle relative to the wall for the growth of the inner layer was 0.93°. The effective origin for δ_m was upstream of the slot face a distance l of about 7 slot heights.

A similar representation is shown in Fig. 12 for the growth of the thickness $\delta_{1,2}$ characteristic of the outer mixing region where the velocity is midway between the peak and the minimum values. These results show that the growth of the thickness $\delta_{1,2}$ was linear in the duct, being the same for each diffuser angle, and also was linear in the diffuser, but varied noticeably with the diffuser total angle. The angle relative to the wall for the growth of the thickness $\delta_{1,2}$ is noted on the figure. Higher injectant flow rates and thus velocities increased the growth of the thickness $\delta_{1,2}$.

The preceding observations of characteristic velocities and thicknesses indicate that the flow in the inner layer of the wall-jet was near similarity in the diffuser for various adverse pressure gradients associated with the different diffuser total angles. This is suggested by the linearity of the growth of the inner layer thickness δ_m and the power law decay of the peak velocity u_m with distance downstream of the slot, typical of wall jets in constant pressure flows, e.g. see the earlier work by Glauert [1] and Seban and Back [6]. However, there were variations in the growth of the thickness $\delta_{1,2}$ characteristic of the outer mixing region which although linear, was dependent upon injection ratio and diffuser total angle, thus indicating non-similar behavior.

5. WALL SHEAR STRESSES AND THE INNER LAYER REGION

Wall shear stresses via the friction velocity $u_\tau = (\tau_w/\rho)^{1/2}$ were estimated to provide a reasonable fit of the velocity data in the viscous sublayer to an appropriate semi-logarithmic representation of the form

$$u^+ = a + b \ln (y^+). \tag{4}$$

In this relation u^+ is the local velocity normalized by the friction velocity u/u_τ, and y^+ is a nondimensional distance normal to the wall, $\rho u_\tau y/\mu$. The density and viscosity were evaluated at the wall condition. Appropriate constants for the von Karman form of this relation are $a = 5.5$ and $b = 2.5$ in the region $y^+ > 30$, and in order to provide a match to the laminar sublayer relation $u^+ = y^+$ to $y^+ = 5$, the constants are $a = -3.05$ and $b = 5$ in the transition layer between y^+ of 5 and 30. The von Karman relation is shown in Figs. 13–15 that span the range of injection ratios for which velocity profiles were measured at a diffuser total angle of 24.9°. However, it is evident in Figs. 13–15 that a number of the profiles tend to lie below the von Karman relation in the viscous sublayer (measurements were made to $y^+ \simeq 5$) and have a reduced slope in this region. Consequently, in these cases the constants a and b were adjusted to $a = 5.0$, $b = 2.1$ in the region $y^+ > 30$ as indicated by the lower curves shown in Figs. 13–15. Best fits in the viscous sublayer were then obtained to this relation and its extension into the transition region.

Observation of the velocity profiles in Figs. 13–15 indicate that reasonable fits were generally achieved in the viscous sublayer. There were some profiles in particular at the largest total diffuser angle $2\theta = 39.9°$ and injection ratio of 2.3 that did not have the usual shape, and therefore, the estimated shear stress was undoubtably in error. Rather large wake components

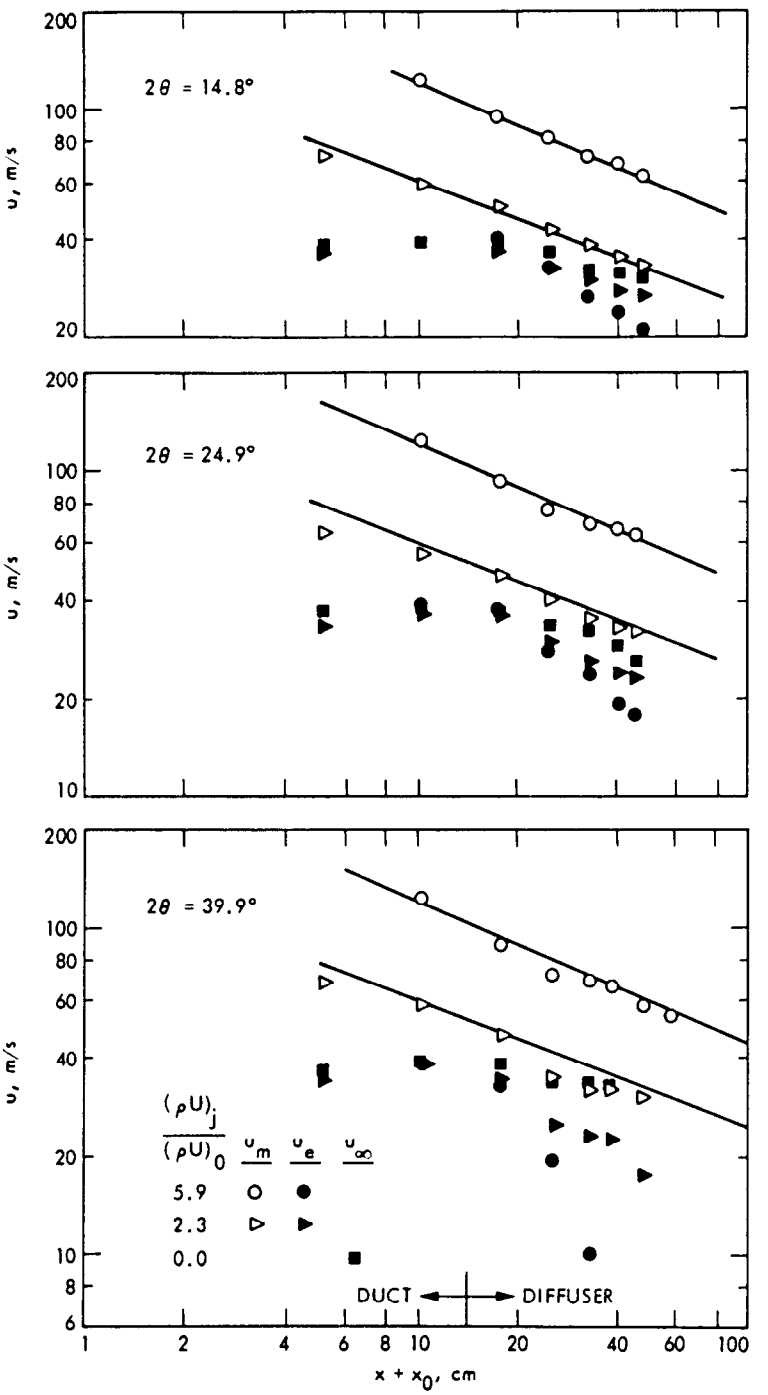

FIG. 10. Variation of characteristic velocities, $2\theta = 14.8$, 24.9 and 39.9°.

[7] in the outer part of the boundary layer are evident in the diffuser with no injection because of the adverse pressure gradient. With injection, velocities diminished in the outer part of the flow because of the lower core flow velocities. At the largest diffuser total angle $2\theta = 39.9°$ and the highest injection ratio of 5.9, local velocities decreased in the outer part of the flow and could not be determined at greater distances from the wall because the flow was reversed in this region as qualitatively depicted in Fig. 9(b).

Wall shear stresses obtained in this manner are shown in Figs. 16–18 at diffuser total angles $2\theta = 14.8$, 24.9 and 39.9°, respectively, as a function of distance along the wall from the slot. The shear decreased along the flow at a particular injection ratio, the solid lines indicating a power law behavior

$$\tau_w \propto (x + x_0)^{-0.8}. \quad (5)$$

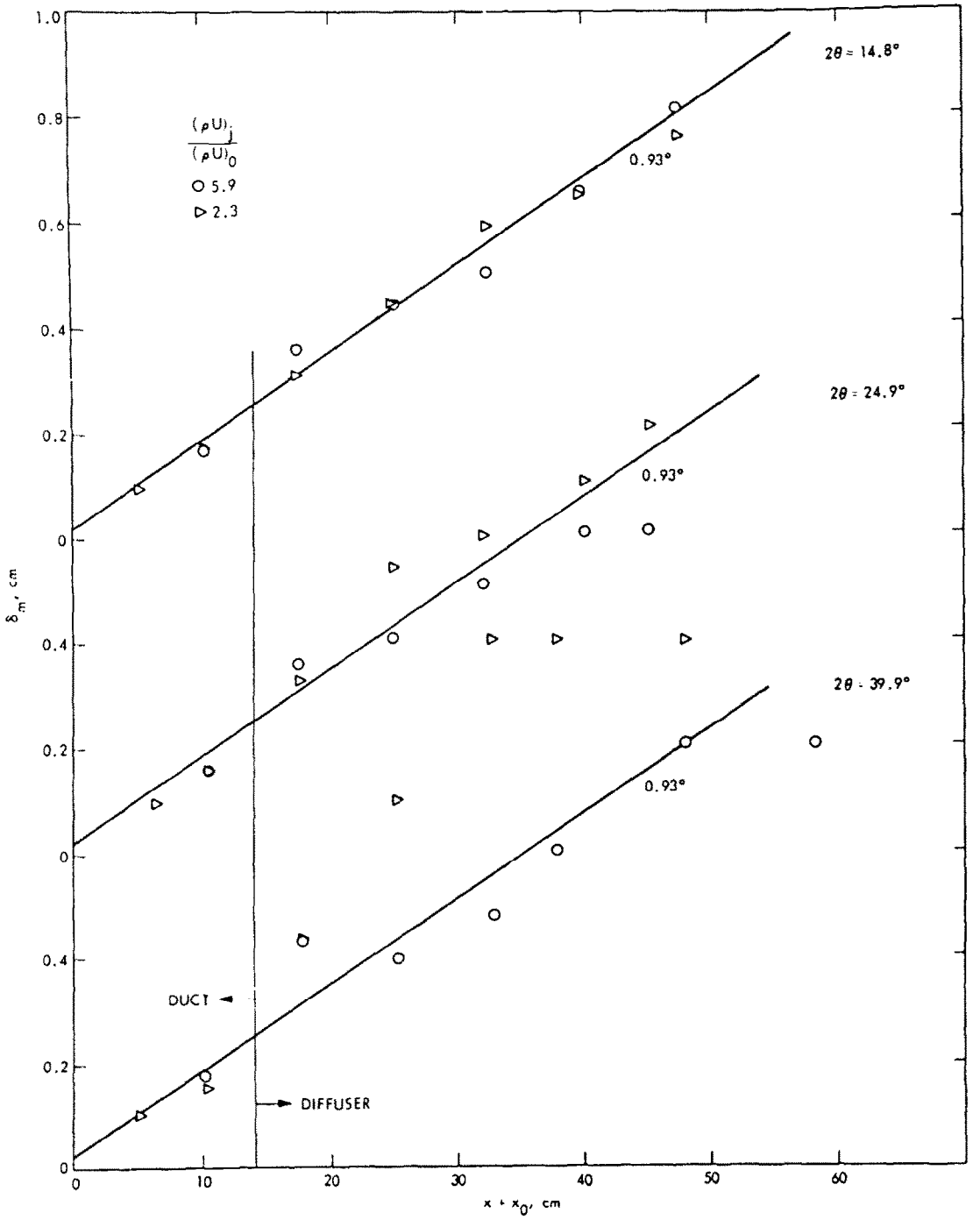

FIG. 11. Variation of inner layer thickness δ_m, $2\theta = 14.8$, 24.9 and 39.9°.

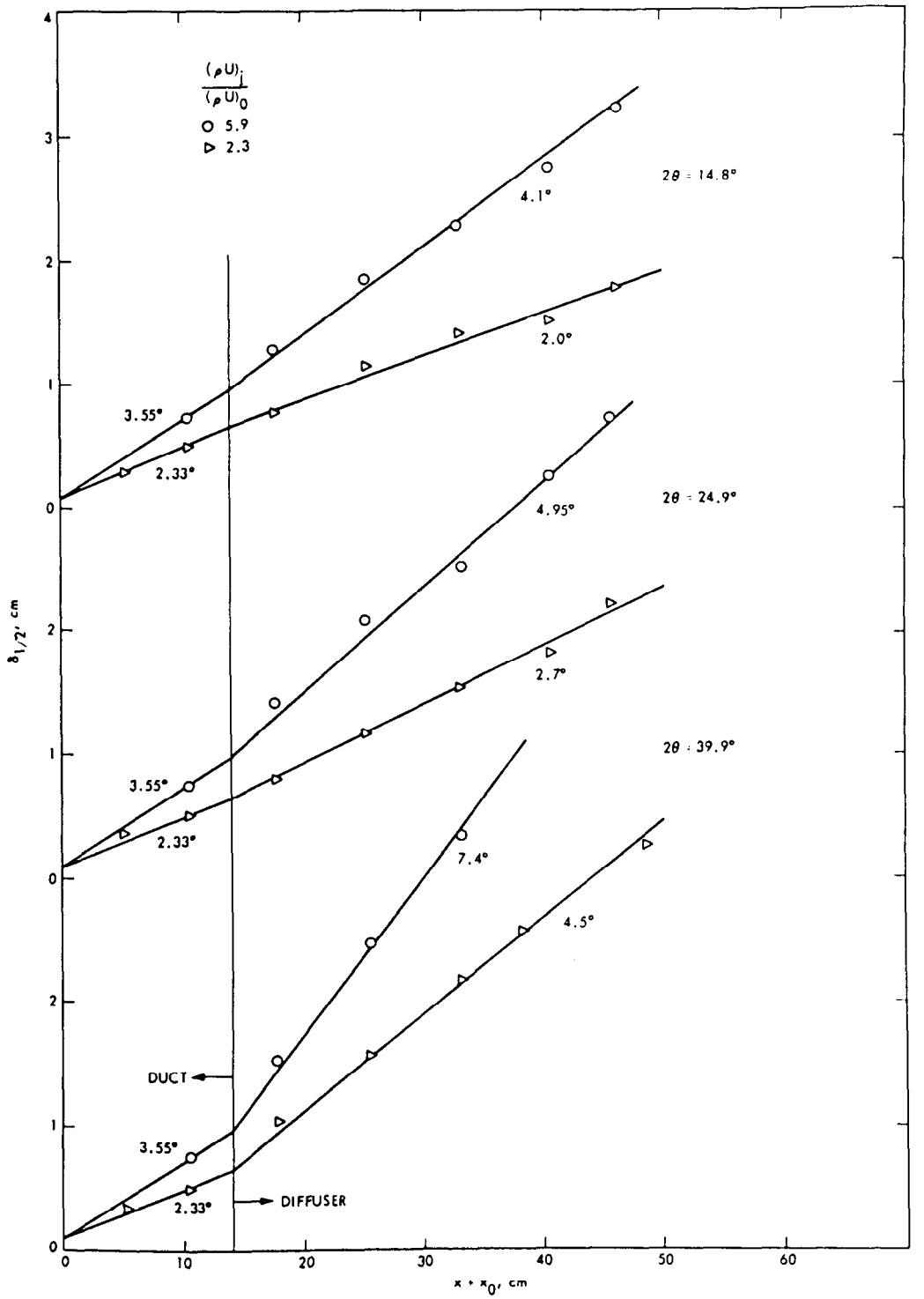

FIG. 12. Variation of the thickness $\delta_{1/2}$, 2θ = 14.8, 24.9 and 39.9°.

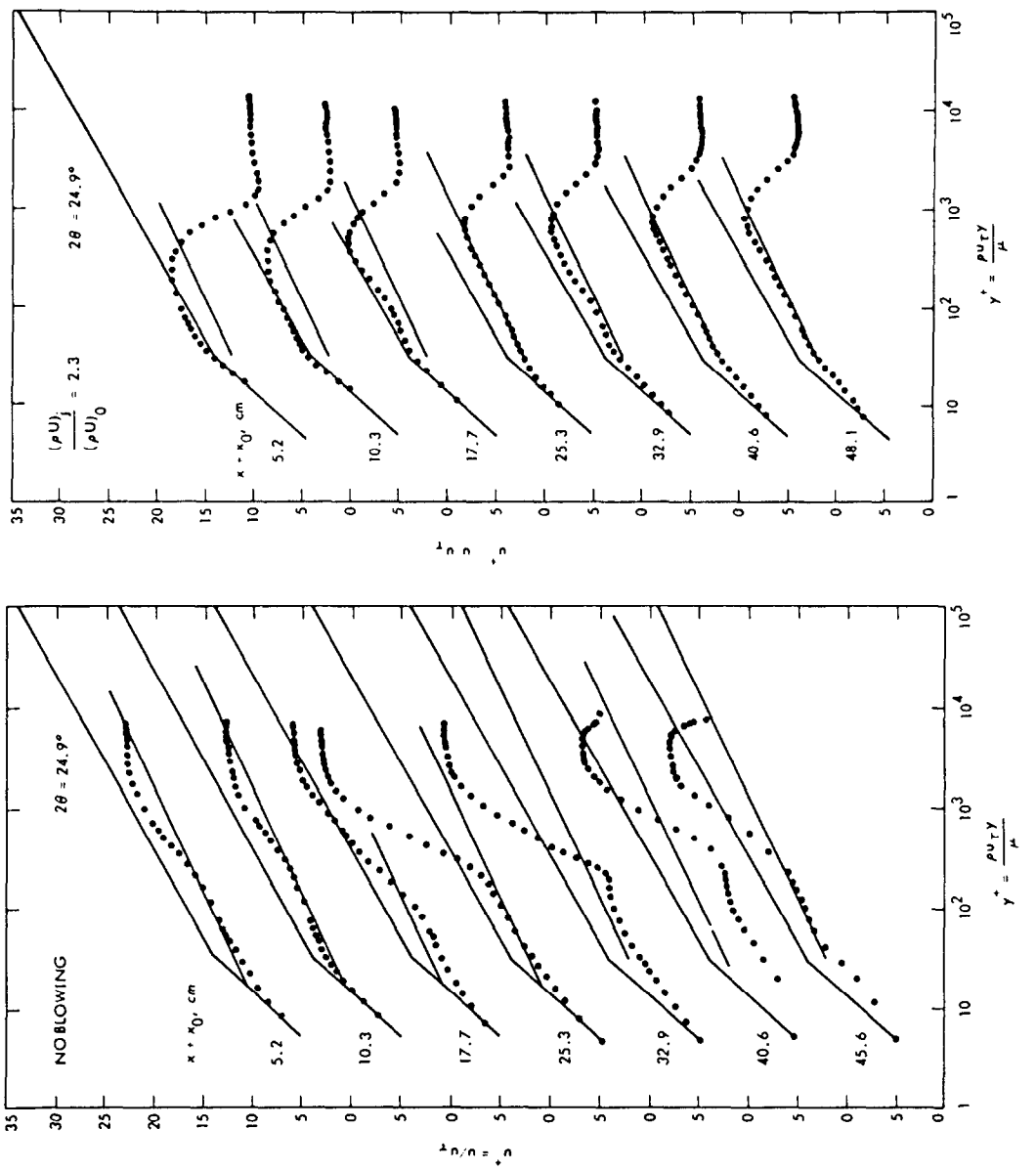

FIG. 13. Velocity profiles on a u^+, y^+ basis, $2\theta = 24.9°$, $m = 0$. FIG. 14. Velocity profiles on a u^+, y^+ basis, $2\theta = 24.9°$, $m = 2.3$.

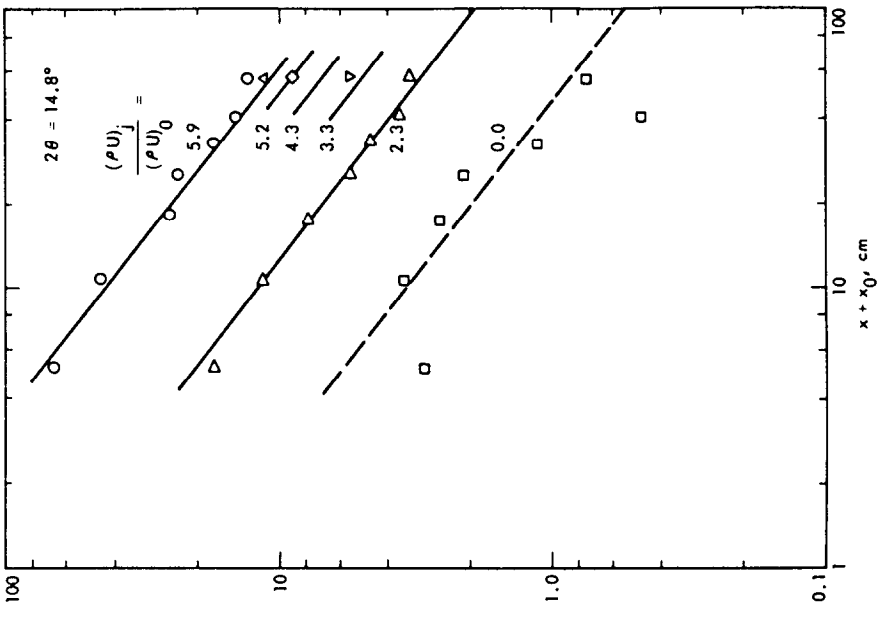

FIG. 16. Wall shear stresses, $2\theta = 14.8°$.

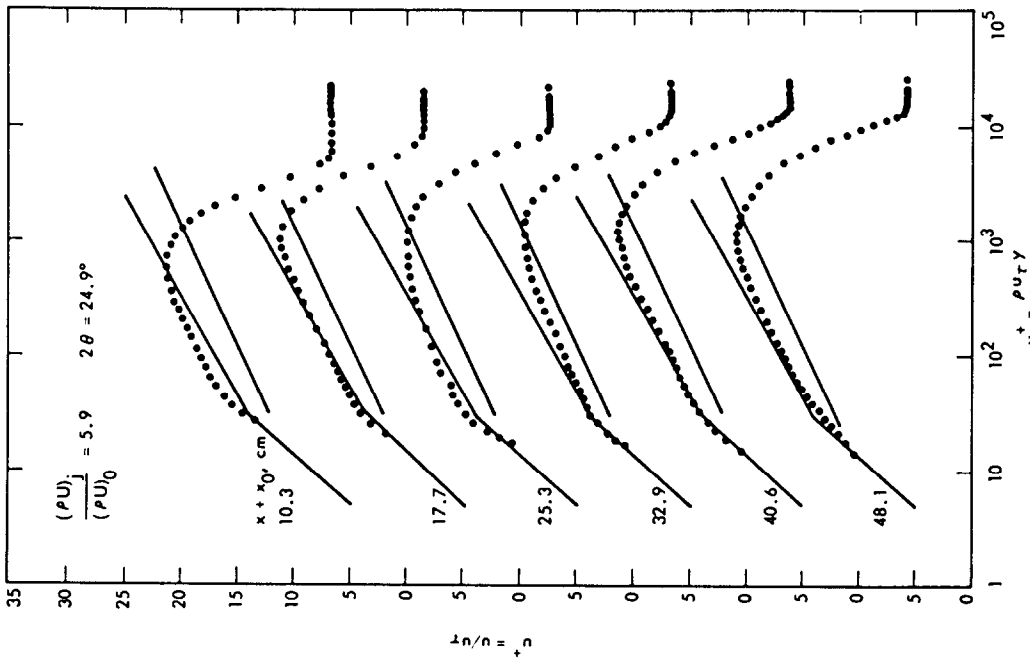

FIG. 15. Velocity profiles on a u^+, y^+ basis, $2\theta = 24.9°$, $m = 5.9$.

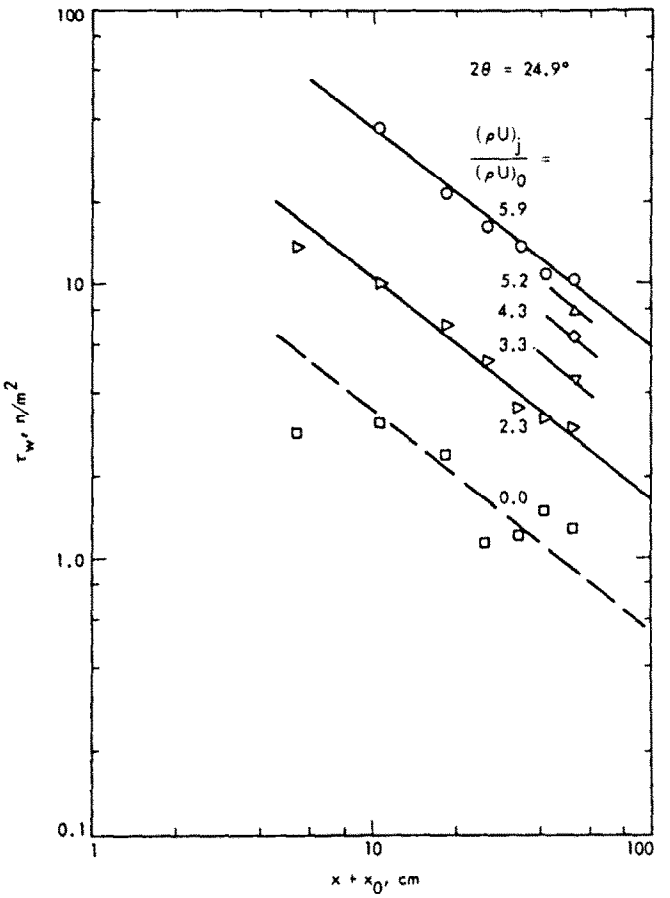

FIG. 17. Wall shear stresses, $2\theta = 24.9°$.

With increasing injection rates the shear stress increased because of higher peak velocities in the wall-jet. In addition to the data acquired all along the wall at injection ratios of 2.3 and 5.9, data for intermediate injection ratios of 3.3, 4.3 and 5.2 obtained from pitot tube traverses at a location near the end of the diffuser are shown also. Comparison of the values shown in Figs. 16–18 indicate that the level of shear stress decreased with increasing diffuser total angle

$$\tau_w \propto \theta^{-0.3}. \tag{6}$$

With no injection there was considerable scatter in the data as indicated in Figs. 16–18. This is expected since there was erratic behavior of the yarn tufts and manometer oscillations which indicated unsteadiness in the flow at all diffuser total angles. As mentioned previously, at the largest diffuser total angle $2\theta = 39.9°$ the flow separated from the upper diffuser plate, and followed along the lower wall (Fig. 9a). The dashed lines shown in Figs. 16–18 are all the same for no injection indicating that the power law dependence of shear stress on distance from the slot

$$\tau_w \propto (x + x_0)^{-0.8}$$

also grossly described this data.

The local shear stress may be expected to scale on the local dynamic pressure $(1/2)\rho u_m^2$ associated with peak velocities in the wall jet. Values of the friction coefficient

$$\frac{c_f}{2} = \frac{\tau_w}{\rho u_m^2}$$

are shown in Fig. 19 as a function of distance along the wall from the effective origin of the wall-jet, $\xi = x + x_0 + l$, in terms of slot heights over the range of diffuser total angles at the highest injection ratio of 5.9. In this representation, the dependence on diffuser total angle is also evident and there appears to be an increase in the friction coefficient in the diffuser. The curve shown is from ref. [6]

$$\frac{c_f}{2} = \frac{0.054}{(U_j s/\nu)^{1/4}} (\xi/s)^{-0.15} \tag{7}$$

which provided reasonable agreement with data for a wall jet without a pressure gradient. Also shown in Fig. 19 is the decay in peak velocity relative to the injection velocity, i.e. u_m/U_j, at the highest injection ratio of 5.9. The ratio of injection to core flow velocity U_j/U_0

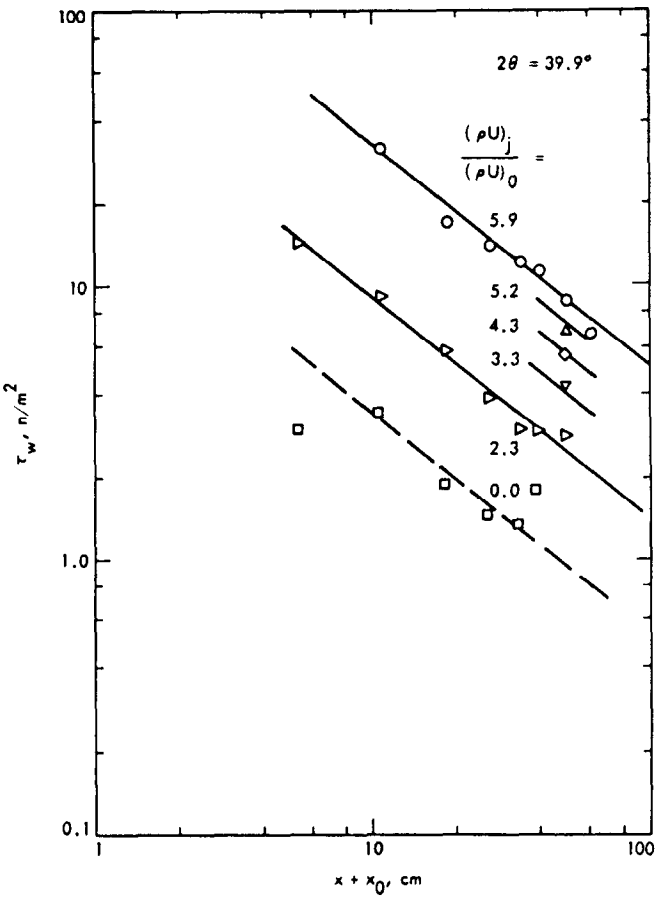

FIG. 18. Wall shear stresses, $2\theta = 39.9°$.

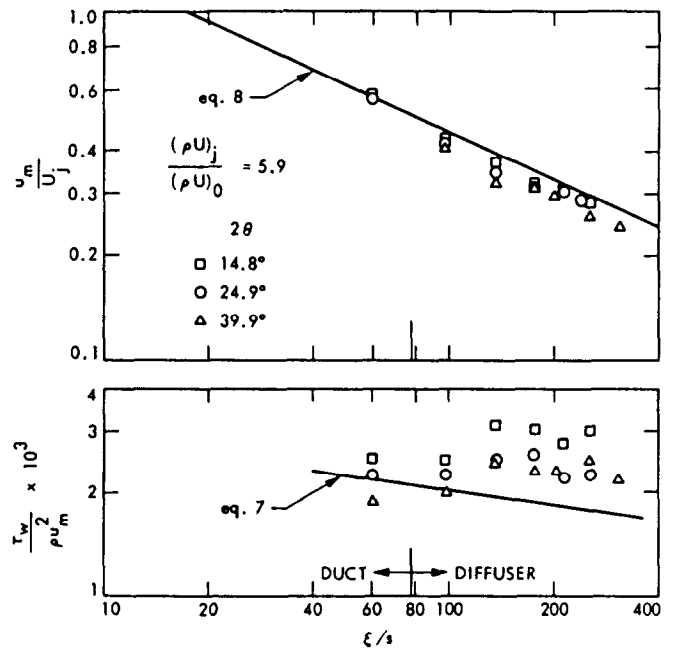

FIG. 19. Wall jet peak velocities and friction coefficients, $m = 5.9$, $2\theta = 14.8$, 24.9 and 39.9°.

estimated by assuming adiabatic flow in the wall jet supply system was about 5.4 for the injection ratio of 5.9, and the slot Reynolds number, $(U_j s/\nu_j) = 3.2 \times 10^4$. The decay of peak velocity in the diffuser was greater than indicated by the empirical curve shown from ref. [6]

$$\frac{u_m}{U_j} = 3.6\,(\xi/s)^{-0.45} \tag{8}$$

for a wall-jet without a pressure gradient, presumably because of the decreasing core flow velocity along the diffuser and increased mixing. Similar trends were found at the lower injection ratio of 2.3; however, since peak velocities u_m became of the same magnitude as the free stream velocity u_∞ (Fig. 10), the velocity ratios u_m/U_j were above the values shown in Fig. 19 for $m = 5.9$, i.e. less decay, and the friction coefficients were above those shown in Fig. 19 for $m = 5.9$, probably because of the lower slot Reynolds number $(U_j s/\nu_j) = 1.02 \times 10^4$ at $m = 2.3$.

6. SUMMARY AND CONCLUSIONS

An experimental study of wall static pressure distributions and mean velocity profiles along a duct and diffuser downstream of wall-jet injection was conducted over a range of diffuser total angles 2θ, from 15 to 40° at injection to core flow mass flux ratios from 0 to 6. Pressure recovery in the diffuser increased with injection ratio and tended to level out more quickly in the diffuser at the larger total angles. At the largest total angle, the static pressure subsequently decreased with distance along the wall at the higher injection rates. Downstream of the wall injection slot, but upstream of the diffuser entrance, the wall static pressure decreased presumably because of the upstream influence associated with the corner at the diffuser entrance.

With wall injection the mean velocity profiles became peaked in the vicinity of the wall associated with the relatively larger injectant than core flow velocities. Peak velocities in the wall-jet then decayed along the flow, and the inner shear layer and outer mixing region grew in thickness along the flow. For the entire range of diffuser total angles and injection ratios, the flow along the lower diffuser plate remained reattached in the vicinity of the wall. At the diffuser largest total angle, the flow separated from the upper diffuser plate with no injection, and the entire flow followed along the lower wall. Also, at the largest total angle and at the highest injection ratio, flow reversal occurred in the core region.

Observations of characteristic velocities and thicknesses indicated that the flow in the inner layer of the wall-jet was near a similarity condition in the diffuser for the various adverse pressure gradients associated with the different diffuser total angles. The growth of the inner layer was linear and the peak velocity in the wall-jet decayed in a power law manner. Both of these features were essentially invariable with injection ratio and diffuser total angle. However, there were non-similar variations in the growth of the thickness, $\delta_{1\,2}$, characteristic of the outer mixing region which although linear, depended upon injection ratio and diffuser total angle.

Wall shear stresses estimated by obtaining reasonable fits of the velocity data in the viscous sublayer to an appropriate sublayer relation, decreased along the flow in a power-law manner because of the associated decay in peak velocities in the wall-jet, and also accordingly, increased with injection ratio. The level of wall shear stress decreased with increasing diffuser total angle.

Comparison to correlation from data obtained for a wall-jet without a pressure gradient indicated greater decay of peak velocity and larger friction coefficients in the diffuser.

Flow unsteadiness was observed with no injection. The flow was apparently more stable with injection.

Information such as obtained in this investigation is of importance in the development of theoretical models capable of predicting the performance of an ejector.

Acknowledgement—This paper presents the results of research carried out at the Jet Propulsion Laboratory, California Institute of Technology under sponsorship of the Naval Air Systems Command MIPR No. N00019-76-MP-67811 by agreement with the National Aeronautics and Space Administration under Contract NAS7-100.

REFERENCES

1. M. B. Glauert, The wall jet, *J. Fluid Mech.* **1**, 625–643 (1956).
2. R. J. Goldstein, Film cooling, in *Advances in Heat Transfer*, (edited by T. F. Irvine, Jr. and J. P. Hartnett, Vol. 7, pp. 321–379. Academic Press, New York (1971).
3. B. R. Ramaprian, Turbulent wall-jets in conical diffusers, *AIAA J.* **11**, 1684–1690 (1973).
4. W. Gracey, W. Lerko and W. B. Russel, Wind-tunnel investigation of a number of total-pressure tubes at high angles of attack. Subsonic speeds, N.A.C.A. Tech. Note No. 2331 (1951).
5. H. A. Becker and A. P. G. Brown, Response of pitot probes in turbulent streams, *J. Fluid Mech.* **62**, 85–114 (1974).
6. R. A. Seban and L. H. Back, Velocity and temperature profiles in a wall jet, *Int. J. Heat Mass Transfer* **3**, 255–265 (1961).
7. D. Coles, The law of the wake in the turbulent boundary layer, *J. Fluid Mech.* **1**, 196–226 (1956).

ETUDE EXPERIMENTALE DES JETS PARIETAUX TURBULENTS EN PRESENCE DE GRADIENTS DE PRESSION ADVERSES DANS UN DIFFUSEUR RECTANGULAIRE

Resume—Une etude expérimentale des distributions de pression pariétale et des profils de vitesse le long d'un tuyau et d'un diffuseur, en aval d'une injection par jet pariétal, est faite pour des angles de diffusion de 15 à 40° et des rapports de flux massiques, à l'injection et en écoulement principal, compris entre 0 et 6. La reconversion de pression dans le diffuseur croît avec le rapport d'injection et décroît avec l'angle du diffuseur. Les pointes de vitesse dans le jet pariétal diminue le long de l'écoulement tandis que la couche interne de cisaillement et la région externe de mélange augmentent d'épaisseur. La couche interne est proche des conditions de similarité, mais des variations non similaires sont trouvées dans la couche externe. Les tensions pariétales estimées dépendent des flux massiques injectés, des distances en aval et de l'angle du diffuseur. Une plus forte décroissance du pic de vitesse et de plus grands coefficients de frottement sont trouvés dans le diffuseur que dans un jet pariétal sans gradient de pression. Pour le plus grand angle du diffuseur et le plus grand rapport d'injection, on observe un retour dans la région centrale.

EXPERIMENTELLE UNTERSUCHUNG EINES TURBULENTEN WANDSTRAHLS BEI ANSTEIGENDEM DRUCK IN EINEM RECHTECKIGEN DIFFUSOR

Zusammenfassung—Die Verteilung des statischen Drucks und das Geschwindigkeitsprofil in einem Rohr und einem Diffusor stromab von einem eingespritzten Wandstrahl wurden experimentell untersucht. Der Diffusor-Gesamtwinkel lag dabei zwischen 15° und 40°, das Verhältnis der Massenstromdichte im Strömungskern und bei der Einspritzung zwischen 0 und 6. Der Druck-Rückgewinn im Diffusor nahm mit dem Einspritzverhältnis zu und mit dem Diffusor-Gesamtwinkel ab. Geschwindigkeitsspitzen im Wandstrahl nahmen entlang des Strömungsweges ab, die Dicke der inneren Reibungsgrenzschicht und des äußeren Mischgebiets wuchsen an. Die innere Schicht gehorchte nahezu den Ähnlichkeitsbedingungen, jedoch kamen in der äußeren Schicht Störungen der Ähnlichkeit vor. Die berechnete Wandschubspannung hing von der Massenstromdichte bei der Einspritzung, der Länge des Strömungswegs und vom Diffusor-Gesamtwinkel ab. Im Diffusor ergaben sich eine schnellere Abnahme der Geschwindigkeitsspitzen und größere Reibungskoeffizienten, als dies nach Korrelationen zu erwarten gewesen wäre, die aus Daten für einen Wandstrahl ohne Druckgradienten ermittelt worden waren. Beim größten Diffusor-Gesamtwinkel und beim höchsten Einspritzverhältnis trat im Kerngebiet Rückströmung auf.

ЭКСПЕРИМЕНТАЛЬНОЕ ИССЛЕДОВАНИЕ ТУРБУЛЕНТНЫХ ПРИСТЕННЫХ СТРУЙ ПРИ ВОЗДЕЙСТВИИ ПОЛОЖИТЕЛЬНЫХ ГРАДИЕНТОВ ДАВЛЕНИЯ В ПРЯМОУГОЛЬНОМ ДИФФУЗОРЕ

Аннотация — Экспериментальное исследование распределений статического давления на стенке и профилей средней скорости по длине канала и диффузора за областью вдува струи через стенку проводилось для диапазона углов раствора диффузора от 15 до 40° при значениях коэффициента вдува, меняющихся в пределах от 0 до 6. Величина восстановления давления в диффузоре увеличивалось с ростом интенсивности вдува и падала с уменьшением угла раствора диффузора. Максимальные значения скорости пристенной струи уменьшались вдоль канала, в то время как толщина внутреннего сдвигового слоя и внешней области смешения увеличивалась. Во внутреннем слое наблюдались почти автомодельные условия, а во внешнем отмечались отклонения от автомодельности. Расчетные значения напряжения сдвига на стенке зависели от потока массы вдуваемого газа, расстояния вниз по потоку и угла раствора диффузора. Для диффузора были получены более сильное снижение максимальной скорости и более высокие значения коэффициента трения, чем в случае пристенной струи без градиента давления. При максимальных значениях угла раствора диффузора и интенсивности вдува в ядре потока отмечалось возникновение возвратного течения.